PAPER

Check for updates

The effect of Si/Al ratio of ZSM-12 zeolite on its morphology, acidity and crystal size for the catalytic performance in the HTO process†

Samira Soltani,[a] Akbar Zamaniyan,*[b] Jafar Towfighi Darian [ID] [a] and Saeed Soltanali [ID] [b]

In this research, ZSM-12 zeolite with six Si/Al ratios (20 to 320) was synthesized by a hydrothermal method and systematically investigated. The physicochemical properties of the synthesized nano zeolites were evaluated and compared by XRD, FE-SEM,ICP-AES, NH_3-TPD, BET, FT-IR, and TGA analyses. The results show that when the Si/Al ratio increases, the amount of microcrystals increases with the dominant competitive phase of cristobalite by decreasing the MTW phase. The catalytic assessment of synthesized zeolites in the (n-hexane to olefins) HTO process in a fixed bed reactor under atmospheric pressure and WHSV equal to 4 h^{-1} at 550 °C was evaluated and various parameters such as selectivity towards light olefins, P/E ratio, production of light alkanes, and aromatic compounds (BTX) were investigated. The result of the n-hexane to olefins process indicated that the presence of cristobalite as an impurity phase strongly affects the activity of the catalysts. The Z80 zeolite, with a Si/Al ratio of 80, corresponds to the pure form of ZSM-12 and exhibits the highest light olefin yield at 52.5%. This zeolite demonstrates superior propylene selectivity (P/E = 1.75) owing to its well-suited pore structure, wide channels, and optimal acidity derived from the MTW zeolite. On the other hand, zeolite Z320 has a lower light olefin yield (19.4%) and a lower P/E (1.1) ratio. In addition, according to the results of the TGA analysis, the content of coke on the Z80 catalyst after the catalytic reaction is much less than other catalysts after the catalytic reactor test.

1. Introduction

The demand for light olefins including ethylene and propylene as primary raw materials in the petrochemical industry is rapidly increasing day by day.[1–4] Catalytic cracking of naphtha due to lower energy consumption and less emission of greenhouse gases can be an effective way to replace the thermal cracking method of naphtha to produce olefins. One of the main issues in catalytic cracking is the type of catalyst used in this process.[5–7]

Therefore, according to the increasing need for light olefins in the industry, it is very important to study and design a catalyst that has a higher selectivity to propylene and secondly toward ethylene. The catalyst has a very decisive role in the direction of the catalytic cracking process, and a slight change in the physicochemical properties of the catalyst can direct the reaction in a certain direction. Among the most active and suitable catalysts for hydrocarbon cracking processes are solid proton-donating acids such as zeolites, which are considered key components of the petroleum industry's cracking catalysts. Zeolites have the ability to increase the selectivity of the process towards desired products (light olefins) due to their shape-selective properties.[8–10] Phase engineering of nanomaterials gives us different ways to design and make new nanomaterials with fresh crystal phases. This is super important for making their physical and chemical properties adjustable and improving how well they work.[11,12]

Zeolite H-ZSM-5 is recognized as one of the best candidates for the catalytic cracking reaction. However, in the catalytic cracking process, the yield of light olefins produced in the cracking of unmodified ZSM-5 is very low and during the long-duration reaction, the catalytic activity and lifetime of this zeolite decrease significantly with the formation of coke. BTX molecules (BTX: benzene, toluene, xylene) are the source of coke in the catalytic cracking reaction. Therefore, to overcome this process's limitations, it is very important to use stable and efficient catalysts. Textural and acidic properties of zeolites can strongly affect the selectivity towards the desired or undesired products.[13,14]

ZSM-12 with the structural type of MTW is a zeolite with a higher amount of silica compared to aluminum and it's composed of the 1D-pore channels with 12 T atoms (T: Si or Al) ring channel system with pore mouths of 5.6 Å × 6.1 Å. Since its pore size is slightly higher than that of ZSM-5, it can be used for

a Department of Chemical Engineering, Tarbiat Modares University, Tehran, Iran
b Catalysis Technologies Development Division, Research Institute of Petroleum Industry (RIPI), Tehran, Iran. E-mail: zamaniyana@ripi.ir

the shape-selective conversion of large molecules, which cannot easily pass into the MFI framework. In addition, due to its acidic properties, ZSM-12 has been suggested as a useful catalyst in many reactions such as isomerization, hydroisomerization, catalytic cracking, and MTO.[15–17] The acid properties of zeolites play a crucial role in hydrocarbon cracking, as catalytic cracking heavily relies on acid catalysis. The amount, strength of acidic sites, and acid types present in zeolites are important factors to consider. While higher acidity in zeolites enhances conversion rates, it can also result in undesirable aromatization reactions. Aromatics, which serve as precursors to coke formation, can lead to catalyst deactivation when their production increases. So, it is very important to modify zeolites with the aim of improving the acid properties in such a way that the amount of coke is produced less so that the catalyst has a higher lifetime and more suitable products are produced. The Si/Al ratio of zeolites plays a crucial role in determining their catalytic cracking performance. This ratio affects the density and strength of acid sites, and optimizing the Si/Al ratio can enhance the overall catalytic activity, propylene selectivity, and catalyst lifetime in hydrocarbon cracking reactions. It is important to note that the catalytic activity of a zeolite in the catalytic cracking process is actually proportional to the concentration of aluminum (which is attributed to strong acid sites).[18–20]

In this work, the effect of six Si/Al ratios on its, acidity, morphology, crystal size, and product distribution in n-hexane cracking of ZSM-12 was studied. Furthermore, different catalysts were characterized by XRD, NH$_3$-TPD, BET, FE-SEM, TGA, and FTIR analyses. Eventually, the function of the synthesized HTO catalysts was examined in a microreactor system.

2. Experimental

2.1 Materials and methods

The materials used in the synthesis of zeolite catalysts were laboratory-grade and of high purity, which include: sodium hydroxide (NaOH, Merck Co.), aluminum sulfate (Al$_2$(SO$_4$)$_3$·18H$_2$O, Merck Co.), Colloidal Silica (40 wt% SiO$_2$, Merck Co.), tetraethyleammonium bromide (C$_8$H$_{20}$NBr, Merck Co.), deionized water, ammonium nitrate (NH$_4$NO$_3$, Merck Co.).

The molar composition of the precursor solution was: $100SiO_2 : xAl_2O_3 : 20TPA : 10Na_2O : 20.5NH_4F : 2000H_2O$ (x = 2.5, 1.25, 0.83, 0.625, 0.3125, and 0.1562. From here on, they are referred to as Z20 (Si/Al = 20), Z40 (Si/Al = 40), Z60 (Si/Al = 60), Z80 (Si/Al = 80), Z160 (Si/Al = 160) and Z320 (Si/Al = 320), respectively. TEABr (tetraethylammonium bromide) was used as the template. After all the materials were mixed properly under 500 rpm at room temperature, the solution was aged for 24 h. The mixture was then transferred to an autoclave equipped with a Teflon liner, in which it was crystallized at 145 °C for 120 h. Then the resulting mixture is washed thoroughly (until reaching neutral pH) with deionized water. After drying at 105 °C overnight, the powder was calcined at 550 °C for 4 h. Finally, ion exchange with 2.0 M NH$_4$NO$_3$ solution was performed two times for 10 min at 85 °C to remove sodium from the zeolite

structure, then it was washed and filtered, and after drying, it was calcined at 550 °C for 4 h.

2.2 Characterization methods

XRD pattern was utilized to identify the zeolite phase and relative crystallinity in 2θ range of 5–80°. The X-ray powder diffraction instrument model X′ Pert Pro (Panalytical Co.) equipped with Cu Kα radiation ($\lambda = 1.5418$ Å) as a generation source of X-ray, with a step size of 0.02° was used for this analysis. The morphology and size of the crystals in the zeolite catalysts are checked using a scanning electron microscopic analysis (FE-SEM) with Sigma VP instrument (ZEISS company, Germany). To identify the structural modification of the prepared samples, the spectrum two IR device manufactured by PerkinElmer, Germany was used. The analysis was performed in the range of wave number 400–4000 with a wavelength of 1 cm^{-1}. The Si/Al ratio of all samples was determined using the Shimadzu ICPE-9820 inductively coupled plasma atomic emission spectrometer (ICP-AES). To calculate the average size of the pores, the pores volume, and the surface area of the zeolites used in this research, the BELSORP MINI model was used. Before carrying out the nitrogen adsorption and desorption tests, the samples were degassed for 3 hours at 300 °C and then the test was performed at 77 K. BET analysis was used to calculate the specific surface area. The total pore volume was obtained from desorption isotherms. The BJH method was used to estimate the volume and size distribution of mesopores, and the t-plot method was used to find the volume and area of micropores. NH$_3$-TPD tests were performed to evaluate the strength of acidic sites of zeolites using a ChemBET-3000 instrument equipped with TCD.

2.3 Catalytic test

After the synthesis of the catalytic samples, the reactor test was performed to investigate the catalytic performance in the catalytic cracking process of n-hexane. Before the reactor test, the powder obtained from calcination was meshed to prevent channelization of the catalyst and proper passage of the feed through different parts of the reactor tube. Fig. 1 shows the fixed bed catalytic reactor. The laboratory catalytic performance evaluation system of the n-hexane to olefin process includes different parts. Firstly, 0.67 g of catalyst was diluted with 0.33 g of quartz, then it was loaded into the reactor. The temperature of the reactor was heated with a temperature gradient of 5 °C min^{-1} to the final temperature of 550 °C under nitrogen flow (as a carrier gas with a flow rate of 40 cm^3 min^{-1}) using an electric furnace equipped with a temperature controller and a thermocouple. To stabilize the conditions at the final temperature, the system remained at the mentioned conditions for 1 h. Then, the n-hexane (feed) flow was injected into the reactor employing a syringe pump with a flow rate of 0.068 cm^3 min^{-1}, under these conditions the value of WHSV was equal to 4 h^{-1}. In the following, the catalytic cracking reaction was carried out by passing the feed through the preheater and reaching the catalytic bed. The output products pass through a condenser and are cooled by a cooling circulator containing
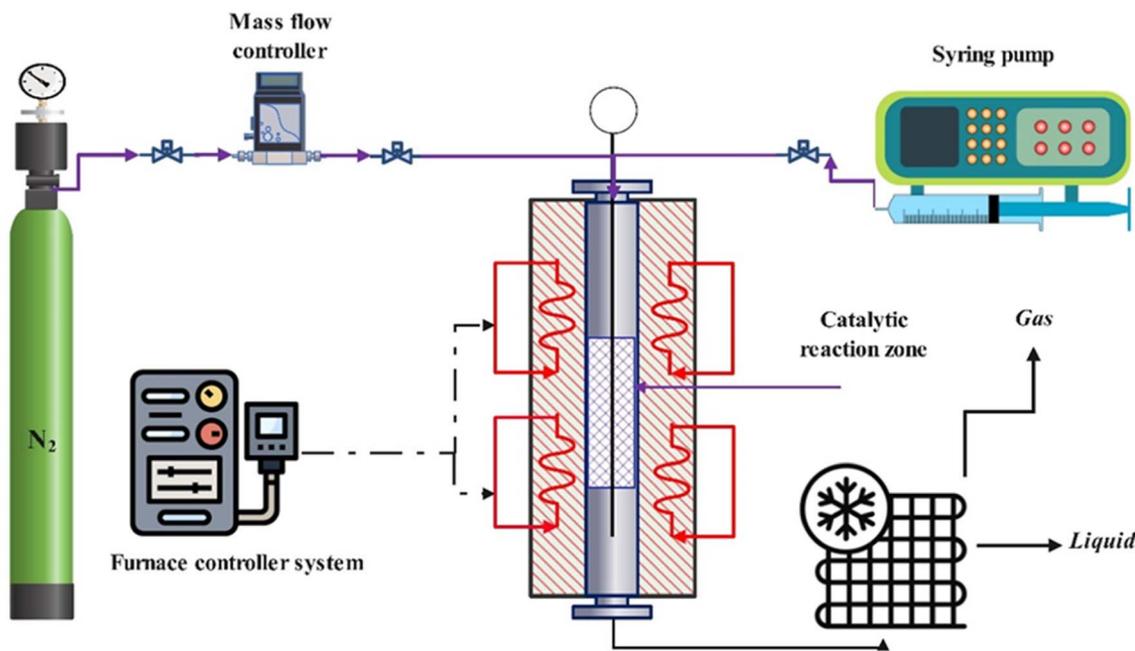
Fig. 1 Schematic diagram of the reactor system used to check the performance of catalysts.

ethylene glycol to a temperature of 1 °C and become two-phase. The gas and liquid products were analyzed by utilization of a gas chromatograph (GC) equipped with a FID and a high-performance liquid chromatograph (HPLC) respectively.

Calculations related to the selectivity to different products and the conversion of *n*-hexane were calculated using the defined eqn (1) and (2). And to investigate the deactivation rate of the catalyst, a percentage decrease in reactant converte (PDRC) was calculated using eqn (3).

$$X_{(n\text{-hexane})} = \frac{(n\text{-hexane})_{\text{inlet}} - (n\text{-hexane})_{\text{out}}}{(n\text{-hexane})_{\text{inlet}}} \times 100\% \quad (1)$$

$$S_{\text{i}} = \frac{n_{\text{i,out}}}{\sum n_{\text{i,out}}} \times 100\% \quad (2)$$

Percentage decrease in reactant convert (PDRC) =
(initial conversion − conversion at certain time)/
initial conversion   (3)

3. Results and discussions

3.1 Characterizations of zeolites

3.1.1 XRD patterns. XRD tool was utilized to investigate the structural properties of the zeolite. The XRD pattern of synthesized zeolites with different ratios of Si/Al = 20–320 is shown in Fig. 2. Different phases of synthesized samples were identified with the reference sample JCPDS. The XRD results show that there is no crystalline phase in the sample synthesized with Si/Al = 20 and it is amorphous. In the sample synthesized with Si/Al = 40, the peaks corresponding to the ZSM-12 sample were identified, and there is no competing phase in the zeolite structure,

but due to the presence of the amorphous phase, the crystallinity and intensity of the peaks are very low. In the sample with Si/Al = 80 ratio, there is no competing and impurity phase and the diffraction pattern of the main peaks of ZSM-12 zeolite with a monoclinic structure based on the intensity of five index peaks at: 7.4°, 8.7°, 18.7°, 20.8°, 23.14° was observed.[21,22] The reflection of plates with miller indices were demonstrated in Fig. 2. According to the Fig. 2, it can be observed that with the increase of the Si/Al ratio from Si/Al = 80–320, competing and impure phases were observed in the structure. In the Z120 sample, were observed ZSM-12 peaks and the main peaks of the ZSM-5 zeolite structure (including five diffraction peaks at 2θ = 7.96, 8.86, 23.08, 23.98, 24.52°).[23–25] Also, the peak related to cristobalite was identified in the structure. To determine the amount of each of the existing phases, using Rietveld refinement with MAUD software and the experimental X-ray diffraction pattern of the synthesized sample was simulated by MAUD. It should be noted that the standard sample was used to calibrate the software. Fig. S1† shows the results of the simulation of the XRD pattern for the Z-80 sample using the Rittold method. Also, the black graph in the lower part of the figure shows that the matching error is negligible and the amount of ZSM-12 phase is reported as the desired and target phase, and competing and impure phases (such as ZSM-5 and cristobalite) are also reported in Table 1. According to the Table 1, with increasing Si/Al ratio from Si/Al = 120–320, competing and impurity phases were observed in the structure. The results of XRD processing with the reference sample JCPDS and MAUD software are shown in Fig. S2.† According to the Fig. S2,† as the increase of Si/Al, the impure phase of crystallobalite increases in the samples, and only in the sample of Si/Al = 80, the pure phase of ZSM-12 was observed.[26–28]
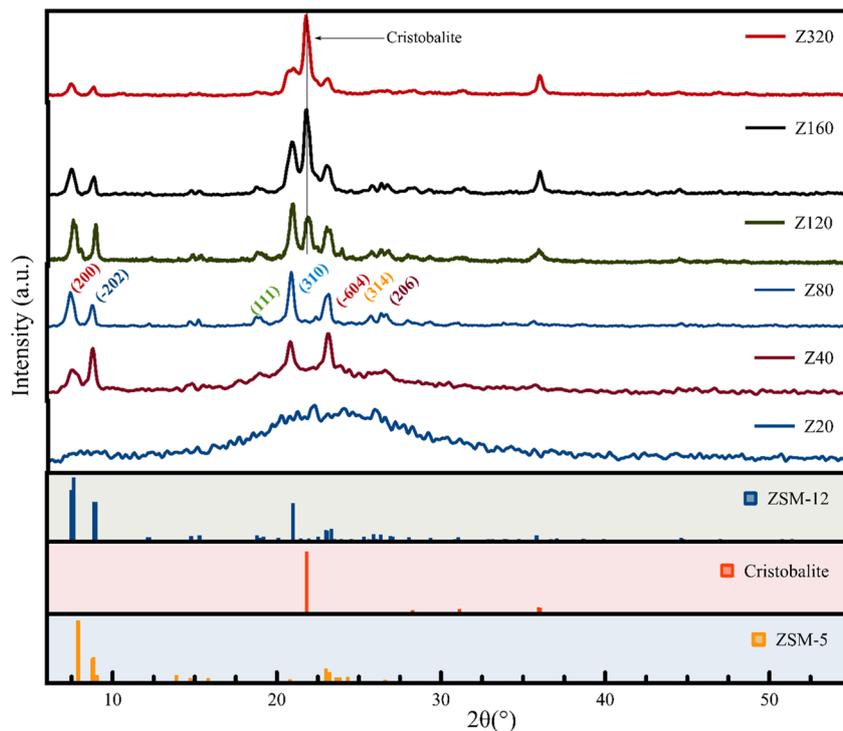
Fig. 2 Effect of Si/Al ratio on X-ray diffraction (XRD).

Table 1 Results from MAUD

ID	ZSM-12	ZSM-5	Cristobalite
Z20		Amorphous	
Z40	>99	Nill	Nill
Z80	>99	Nill	Nill
Z120	68.5	10.8	20.7
Z160	58.5	Nill	41.5
Z320	48.5	Nill	51.5

3.1.2 FTIR spectra. Chemical groups and bonds in the substance are identified using FTIR spectroscopy.[29,30] The FTIR spectrum of Z40, Z80, and Z120 samples is shown in Fig. 3 FTIR vibrations can be classified into two categories: internal vibrations and external vibrations. The internal vibrations are specific to the vibrations of TO_4 tetrahedrons and they change slightly in the vibrational spectrum of all zeolites depending on the type of zeolite network. The external vibrations depend on the topological structure of the studied zeolite and show the formation of bonds between TO_4 with a certain structure. According to the reports in the literature, the FTIR spectrum of ZSM-5 structures has five peaks at 460, 548, 802, 1094, and 1225 cm^{-1} and the FTIR spectrum of zeolite ZSM-12 has seven peaks at 470, 543, 580, 645, 786, 1090, and 1225 cm^{-1}.[27,31] The presence of vibrations at the mentioned wavenumbers confirms the ZSM-5 (MFI) and ZSM-12 (MTW) structures.[32] Since the synthesized zeolitic catalysts have two phases of ZSM-5 (lower) and ZSM-12(higher), the peaks of the MTW phase are more intense in the spectrum of the samples which can be attributed

to the asymmetric and symmetric external vibrations of the zeolite framework, respectively.[33]

The peak around 3500 cm^{-1} is ascribed to structurally hydroxyl groups usually acts as an acid site. According to the Fig. 3 the absorption peak intensity of the Z80 sample in 3500 cm^{-1}, is higher than other samples, which indicates the presence of more acidic sites in this sample.[33,34] This conclusion is further evaluated by NH$_3$-TPD analysis in the following.[22] Also, in the IR spectrum, the ratio of vibration intensity at the wavenumber 550 cm^{-1} to 450 cm^{-1} indicates the degree of crystallinity. The higher of this ratio is the greater the crystallinity of the sample.[35–37] The ratio number mentioned for the Z80 sample has the highest value, which indicates the greater crystallinity of this sample compared to other samples. The peak at the wavenumber of 682 cm^{-1}, indicates the presence of cristobalite, which is more intense in the Z120 sample than the other samples, which is due to the impurity phase of cristobalite in this sample.

3.1.3 FE-SEM images. Fig. 4 displays typical field emission scanning electron microscope (FE-SEM) images of the MTW samples, each with varying Si/Al ratios. The FE-SEM findings reveal that the Si/Al ratio plays a crucial role in determining the morphology of the synthesized compounds. Specifically, in Fig. 4(a), Z20 exhibits a combination of large bulk structures and irregularly shaped crystals of varying sizes. Fig. 4(b) shows the FE-SEM images related to the synthesized ZSM-12 sample with Si/Al ratio = 80. According to the sample images, the nanocrystals are completely uniform, with the same morphology and a coffin-like shape with rough external
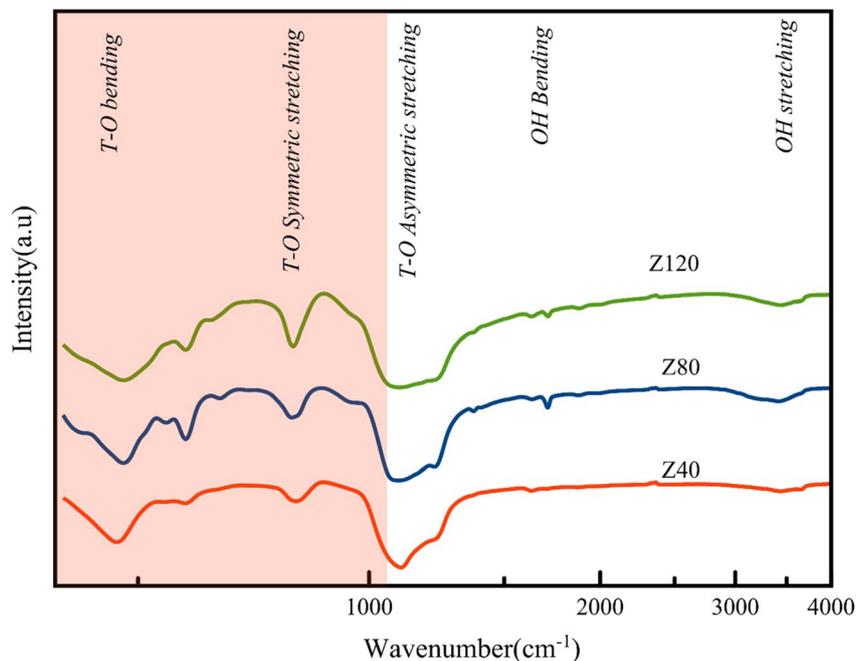
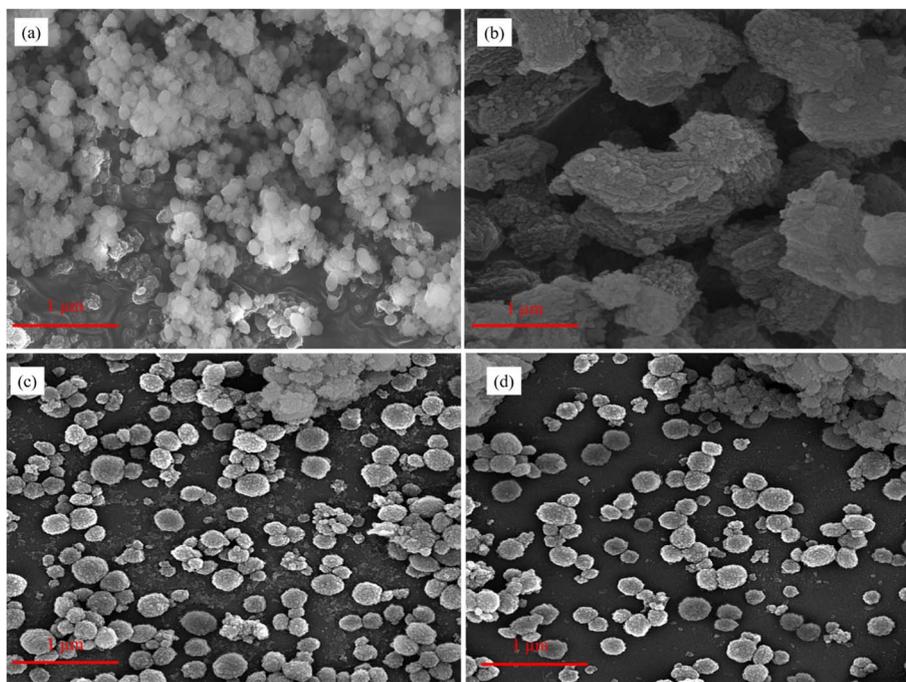**Fig. 3** FTIR technique with changing Si/Al ratio.

Fig. 4 FESEM images of (a) Z-20, (b) Z-80, (c) Z-160, (d) Z-320.

surfaces. The size of synthesized zeolite particles is below 100 nm. It can also be claimed that the synthesized zeolite is nano zeolite. Mixed morphologies were observed at Si/Al ratios of 160 and 320. Both irregular crystal and coffin-like shaped-agglomerates were obtained. Fig. S3,† presents the images obtained from FE-SEM of the synthesized Z-80 at various magnifications.

3.1.4 Nitrogen adsorption and desorption tests. The results of N_2 adsorption and desorption tests including pore volume, BET surface area, average pore size, and micropore area are given in Table 2 and Fig. 5. All the isotherms of the synthesized samples are of type IV with hysteresis loop of type H3, which can be confirmed by the available sources. Based on hysteresis loops, the pores in all samples are parallel plates. Also, the

Table 2 BET analysis results of zeolite and chemical composition of zeolite

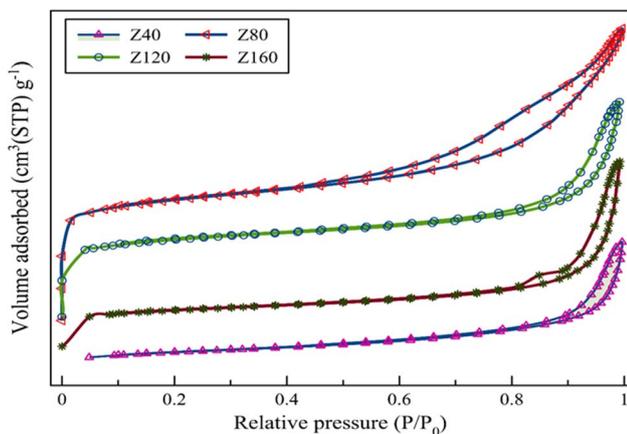| Samples	Z40	Z80	Z120	Z160
Specific surface area (m^{-2} g^{-1})	65.5	309.3	228.2	147.2
Surface area micro (m^{-2} g^{-1})	27.7	216.4	157.3	109.2
Pore volume (cm^3 g^{-1})	0.01	0.12	0.08	0.04
Pore diameter (nm)	4.6	1.5	1.4	1.4
Si/Al (measured by ICP-AES)	39.84	79.65	119.31	159.15

Fig. 5 Nitrogen isotherms of synthesized zeolites.

hysteresis loop near the integral point of high pressure has moved up vertically, which indicates the open structure of hierarchical zeolite pores. In the Z80 sample, the presence of a hysteresis loop of N_2 adsorption and desorption isotherms in the relative pressure range = 0.1–0.4, which indicates a mesoporous structure, while in other samples, it starts from a relative pressure of about 0.7. Due to the low crystallinity and the presence of amorphous phase, the Z40 sample has the lowest specific surface area and the lowest pore volume, whereas the Z80 sample has the highest specific surface area and the highest pore volume due to its high crystallinity according to XRD analysis. Higher specific surface area increases the accessibility of active acid sites to normal hexane feed molecules. According to Table 2, the increase in the ratio of Si/Al, the specific surface area, and the pore volume decrease compared to the Z80 sample, which is probably due to the change in the interaction of aluminum and silica in the zeolite structure.[23,38,39] According to these results, it can be stated that changes in the Si/Al molar ratio have a great effect on the surface and pore structure of zeolite. Additionally, the amount Si/Al ratio was measured using ICP-AES and the results are shown in Table 2.

3.1.5 NH₃ temperature programmed desorption. The results of the NH₃ temperature programmed desorption (NH_3-TPD) analysis are shown in Fig. 6. NH_3-TPD analysis was used to determine the strength and density of zeolite acid sites. In this way, the amount and strength of acidic sites are determined by using the area under the peak of the NH_3-TPD profile and the location of the peaks, respectively.[40,41] As shown in Fig. 6 the profiles of the samples have three main regions included: low

temperature (LT), medium temperature (MT), and high temperature (HT), which indicate weakly acidic sites, medium acidic sites, and strong acidic sites, respectively.[42,43] The first peak of ammonium desorption appears at 180–200 °C, which is attributed to weak acid sites (LT), the second peak of ammonium desorption appears at 250–310 °C, which is attributed to moderately acidic sites (MT), and the third peak of ammonium removal appears at 400–360 °C, which is attributed to strong acidic sites (HT). The amount of different acidic sites of each peak for each sample was calculated according to the obtained data and shown in Table 3. According to Table 3, the Z80 catalyst has the highest amount of weak acid sites. In the Z120 catalyst, peaks related to medium acid sites were not observed. According to Table 3, at high Si/Al ratios, the acidity reaches a maximum and decreases again.[33,35] According to the results, it can be stated that changes in the Si/Al ratio have a significant effect on the amount and distribution of acidic sites of the catalyst, but at the same time, the trend of changes in acidity with a change in the Si/Al ratio cannot be predicted in all cases. Also, any factor that changes the Si/Al ratio in the structure of zeolite affects the catalytic properties of zeolite.

3.2 Catalytic assessment of samples

To clarify the reactor performance of the catalysts and investigate the effect of Si/Al ratio on the catalytic performance, HTO tests were performed at 550 °C, under atmospheric pressure the value of WHSV was equal to 4 h^{-1}. The results of the reactor evaluation of catalysts are summarized in Fig. 7 and Table 4 and the selectivity toward light olefins, the production rate of light alkanes, the stability rate, the P/E ratio, and the production rate of aromatic compounds (BTX) have been investigated. According to Fig. 7 and Table 4, the Z320 sample has the lowest *n*-hexane conversion and the Z80 sample has the highest conversion, which is almost 100%, indicating that all the *n*-hexane has been converted into a product. Also, the Z80 catalyst has the best result in terms of yield of light olefins, in the following, the influence of the characteristics of the synthesized zeolites will be investigated.

3.2.1 Effect of physical and chemical properties by changing Si/Al ratio on catalyst performance. As stated in Section 3.1.1, increasing the Si/Al ratio increases the presence of impure and competing phases in the samples, which strongly affects the catalyst activity. The amount of yield of light olefins for the Z80 sample is higher than other samples. Due to its high crystallinity, and high amount of acidic sites, this sample has a greater tendency to produce light olefins, especially propylene. According to the composition of products in Table 4, the selectivity towards light olefins for Z80 and Z120 samples is about 52 and 57%, respectively. While the selectivity to the sum of C1–C4 for the mentioned samples is 43 and 41%, respectively, which shows that the selectivity to products in the Z80 sample tends towards saturated hydrocarbon products. The production rate of alkenes ($C4^+=$) and ($C3^+=$) for the Z80 sample is more than the other samples, which can be attributed to the appropriate number of strong acid sites, which are responsible for converting to light olefins, especially
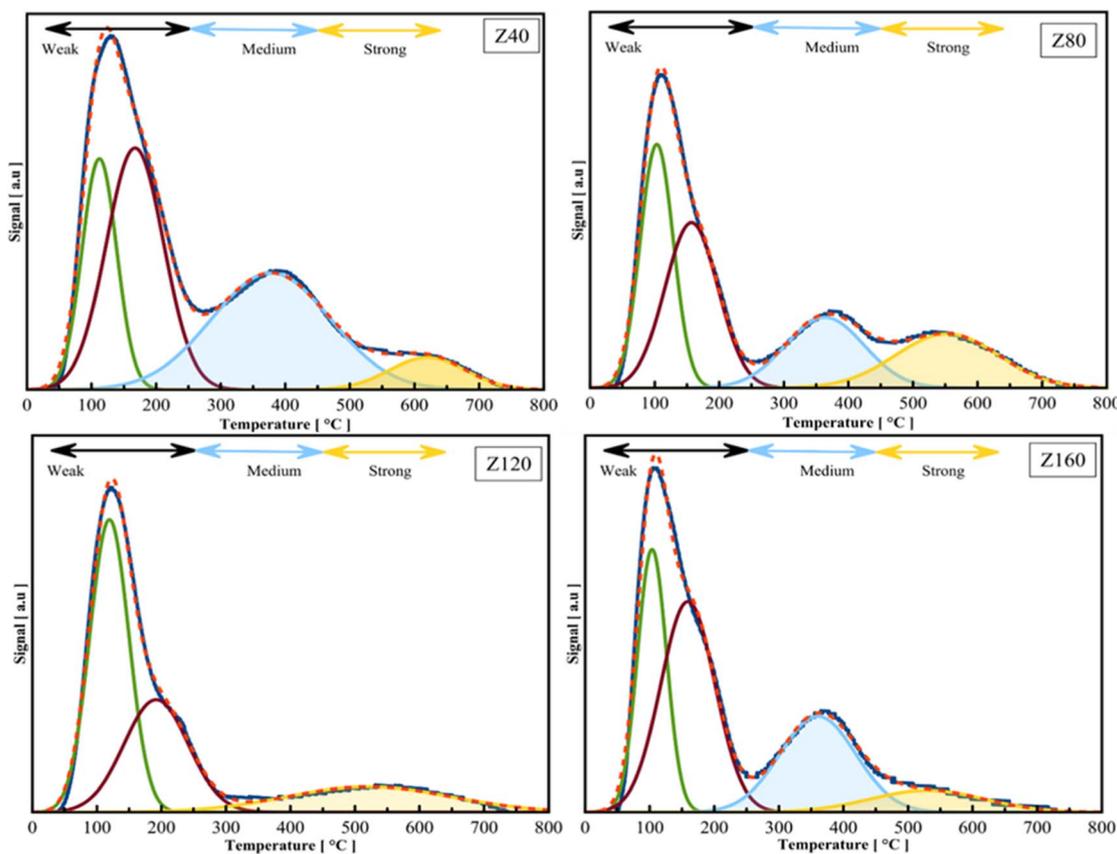
Fig. 6 NH$_3$-TPD analysis results with changing Si/Al ratio.

Table 3 The results of the acidity test

Sample ID	Acidity concentration (mmol NH$_3$ per g)				
	Weak	Medium	Strong	Total	S/W
Z40	0.22	0.14	0.06	0.42	0.27
Z80	0.35	0.1	0.08	0.53	0.22
Z120	0.25	0.0	0.07	0.32	0.28
Z160	0.13	0.06	0.02	0.21	0.15

propylene.[44–46] According to the research done, an excessive increase of strong acid sites leads the reaction to side reactions.[47] The Z80 sample has the highest P/E (=1.75). In fact, this sample shows more selectivity to propylene due to its large diameter channels, suitable acidity, and medium pore structure. Also according to eqn (3) and Fig. S4† PDRC parameter, which is the percent decrease reactant conversion and indicates the stability of the catalyst. Z80 catalyst has the lowest PDRC value and this sample is deactivated with a lower speed and slope than other samples and has higher stability. According to the obtained results, it can be stated that the Z80 catalyst has the highest acidity, the highest yield of light olefins especially propylene, maximum stability, and the best performance compared to other samples. In addition to the acidity, the high crystallinity of the Z80 sample helps the penetrate of molecules.

The high crystallinity structure and more open pores can promote the catalytic activity with facilitate reactant diffusion improve mass transfer and molecular diffusion in pores.[33] Also, reduce the length of the diffusion path and facilitate the diffusion of products through the pores, which leads to an increase in the activity of the zeolite. On the contrary, larger and denser particles increase the length of the diffusion path and make it difficult for products to spread. As a result, the large diffusion path length can lead to the progressive second reactions of light products (olefin) (such as oligomerization and hydrogen transfer), which lead to the production of large hydrocarbons and pore blocking, which can reduce the activity of the zeolite. In addition, according to Fig. 9, the higher concentration of Z80 acidic sites increases the reaction speed and catalyst activity. The relationship between the Si/Al ratio and selectivity towards propylene and acidity is shown in Fig. 8. According to the results, with the increase of Si/Al, the amount of total acidity decreases, as a result, the amount of selectivity C3 decreases. The decrease in the selectivity of olefin, especially ethylene, and propylene, with the reaction time can be attributed to the diffusion resistance of molecules due to the blockage of pores by coke deposits and heavy hydrocarbons. In other words, when many strong acid sites are blocked by heavy particles, the selectivity of light olefins becomes weaker while side reactions increase, such as hydrogen transfer reactions and higher hydrocarbons, which are further investigated in TGA
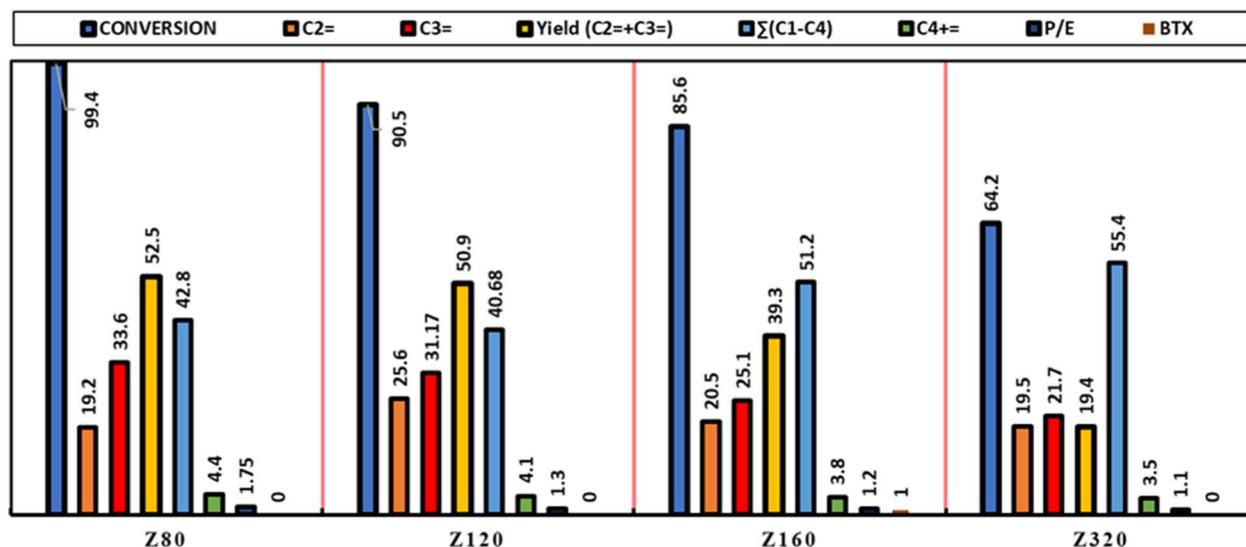
Fig. 7 Reactor test results.

Table 4 The results of the reactor test in zeolites with different Si/Al ratios

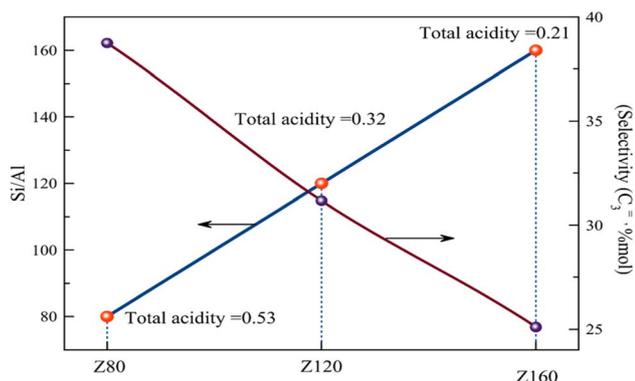| Samples	Si/Al	X (%)	$C_2^=$ (% mol)	$C_3^=$ (% mol)	Yield ($C_2^=$ + $C_3^=$)	$\sum(C_1-C_4)$	$C_{4+}^=$	P/E	PDRC	BTX
Z80	80	99.4	19.2	33.6	52.5	42.8	4.4	1.7	1.0	Nill
Z120	120	90.5	25.6	31.17	50.9	40.68	4.1	1.3	13.5	Nill
Z160	160	85.6	20.5	25.1	39.3	51.2	3.8	1.2	14.1	1.0
Z320	320	64.2	19.5	21.7	19.4	55.4	3.5	1.1	39.4	Nill

Fig. 8 Relationship between Si/Al ratio and selectivity towards propylene and acidity.

analysis.[26,32,48,49] Moreover, we also compared the catalytic performance of our material with the catalysts reported in the literature, as shown in Table 5.

3.3 Evaluation of the spent catalysts

3.3.1 Thermogravimetric analysis. The amount of coke deposited on the spent catalysts was checked by TGA analysis. The results of the TGA analysis are shown in Fig. 9. One of the important and effective factors in the deactivation of the catalysts used in the cracking process is the process of coke deposition on the catalysts during the cracking process, which causes

the reduction of active acid sites to carry out the reaction. The amount of deposited coke depends on strong acid sites, catalytic reactivity, density of active acid sites, catalyst architecture and morphology, *etc.* Based on the research in the literature, the amount of weight loss in the temperature range of 40–250 °C is related to the loss of moisture and dust in the pores and surface of the samples, and the amount of weight loss in the temperature range above 250 °C is related to the burning of coke. Coke deposits are mainly formed through olefin polymerization during the dehydrogenation reaction, which can be channelized in acidic sites.[51,52] According to Fig. 9, the amount of deposited coke is observed in the order of Z120 > Z160 > Z80. The Z120 sample has the highest amount of coke deposited and the sample Z80 has the lowest amount of coke. The Z80 sample has a larger average pore diameter than the other samples, which prevents the blocking of large hydrocarbons inside the zeolite pores and deposition in acidic sites. In addition, due to the shorter diffusion pathway, access to acidic sites in pores increases, which reduces mass transfer limitations. Therefore, less amount of coke is deposited on it. Also, according to the obtained data of NH$_3$-TPD analysis in this sample, the number of acidic sites with medium strength is more than the number of acidic sites with strong strength. According to the sources, it can be stated that the higher number of acid sites with moderate strength than the number of acid sites with strong strength prevents the formation of coke and heavy products during side reactions, thus increasing the activity of the catalyst.[10]

Table 5 The documented performance of zeolite, in the literature

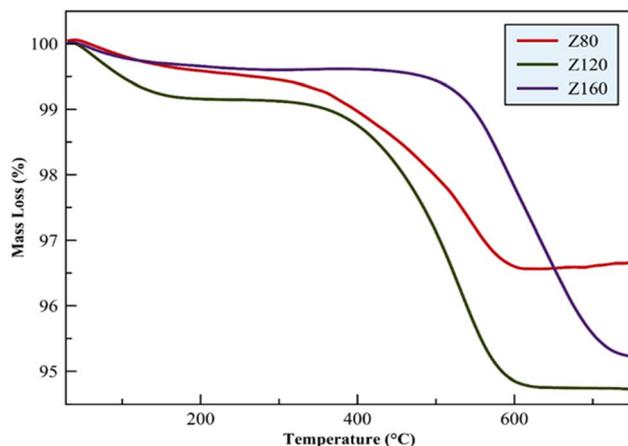| No.	Catalysts	Temp. (C)	WHSV (h^{-1})	Conversion (%)	P/E	Yield ($C_2^=$ + $C_3^=$) (%)	Si/Al	Ref.
1	S1 (ZSM-12)	650	3.6	60	1.48	34.7	120	31
2	ZSM-5	550	4	95.21	2.05	43.37	200	50
3	Parent (ZSM-5)	550	4	94.8	1.48	47.97	120	24
4	Z100 (ZSM-5)	600	6	99	1.21	64.0	100	10
10	Z80	550	4	99.4	1.7	52.5	80	This work

Fig. 9 TGA profiles of spent catalysts.

4. Conclusion

In this research, the synthesis of ZSM-12 zeolite in different Si/Al ratios was investigated and then the synthesized zeolites were evaluated and compared by using different analyses and were evaluated in the HTO process. Various parameters such as selectivity towards light olefins, production of light alkanes and aromatic compounds (BTX) and P/E ratio were investigated. The results of the XRD pattern showed that the increase of Si/Al leads to an increase in the formation of competing phases in the zeolite structure. The presence of cristobalite as an impurity phase strongly affects the activity of the catalyst. The Z80 zeolite, with a Si/Al ratio of 80, corresponds to the pure form of ZSM-12 and exhibits the highest light olefin yield at 52.5%. This zeolite demonstrates superior propylene selectivity (P/E = 1.75) owing to its well-suited pore structure, wide channels, and optimal acidity derived from the MTW zeolite. On the other hand, zeolite Z320 has a lower light olefin yield (19.4%) and a lower P/E (1.1) ratio. In addition, according to the results of TGA analysis, the Z80 catalyst has high thermal stability and the amount of coke deposited on this catalyst is much less than other catalysts after the catalytic reactor test. The reason for this can be attributed to optimal physical and chemical properties.

Conflicts of interest

There are no conflicts to declare.

References

1 S. M. Sadrameli, *Fuel*, 2016, **173**, 285–297.
2 F. Gorzin, J. T. Darian, F. Yaripour and S. M. Mousavi, *J. Porous Mater.*, 2019, **26**, 1407–1425.
3 V. Blay, B. Louis, R. Miravalles, T. Yokoi, K. A. Peccatiello, M. Clough and B. Yilmaz, *ACS Catal.*, 2017, **7**, 6542–6566.
4 O. Bortnovsky, P. Sazama and B. Wichterlova, *Appl. Catal., A*, 2005, **287**, 203–213.
5 O. Muraza, I. A. Bakare, T. Tago, H. Konno, T. Taniguchi, A. M. Al-Amer, Z. H. Yamani, Y. Nakasaka and T. Masuda, *Fuel*, 2014, **135**, 105–111.
6 K. Urata, S. Furukawa and T. Komatsu, *Appl. Catal., A*, 2014, **475**, 335–340.
7 X. Gao, Z. Tang, D. Ji and H. Zhang, *Catal. Commun.*, 2009, **10**, 1787–1790.
8 A. Yamaguchi, D. Jin, T. Ikeda, K. Sato, N. Hiyoshi, T. Hanaoka, F. Mizukami and M. Shirai, *Fuel Process. Technol.*, 2014, **126**, 343–349.
9 Y. Bai, G. Zhang, D. Liu, Y. Zhang, L. Zhao, J. Gao, C. Xu, Q. Meng and X. Gao, *Appl. Catal., A*, 2021, **628**, 118399.
10 M. R. Sakha, S. Soltanali, D. Salari, M. Rashidzadeh and P. H. Tabrizi, *J. Solid State Chem.*, 2021, **301**, 122342.
11 Z. Liu, K. Nie, X. Qu, X. Li, B. Li, Y. Yuan, S. Chong, P. Liu, Y. Li and Z. Yin, *J. Am. Chem. Soc.*, 2022, **144**, 4863–4873.
12 B. Li, K. Nie, Y. Zhang, L. Yi, Y. Yuan, S. Chong, Z. Liu and W. Huang, *Adv. Mater.*, 2023, **35**, 2303285.
13 Y. Nakasaka, J. Nishimura, T. Tago and T. Masuda, *Chem. Eng. J.*, 2015, **278**, 159–165.
14 S. Mintova, M. Jaber and V. Valtchev, *Chem. Soc. Rev.*, 2015, **44**, 7207–7233.
15 Q. Wang, Z.-M. Cui, C.-Y. Cao and W.-G. Song, *J. Phys. Chem. C*, 2011, **115**, 24987–24992.
16 P. Dugkhuntod, T. Imyen, W. Wannapakdee, T. Yutthalekha, S. Salakhum and C. Wattanakit, *RSC Adv.*, 2019, **9**, 18087–18097.
17 K. S. Yoo, S. Gopal and P. G. Smirniotis, *Ind. Eng. Chem. Res.*, 2005, **44**, 4562–4568.
18 Y. Wang, T. Yokoi, S. Namba, J. N. Kondo and T. Tatsumi, *Appl. Catal., A*, 2015, **504**, 192–202.
19 J. Pérez-Ramírez, D. Verboekend, A. Bonilla and S. Abelló, *Adv. Funct. Mater.*, 2009, **19**, 3972–3979.
20 X. Zhu, S. Liu, Y. Song and L. Xu, *Appl. Catal., A*, 2005, **288**, 134–142.

21 S. Wang, C. Wang, H. Liu, D. Wang, X. Wang, L. Yang, P. Li and Z. Tian, *Microporous Mesoporous Mater.*, 2023, **348**, 112364.

22 S. Li, B. Mezari, H. Wu, N. Kosinov and E. J. M. Hensen, *Fuel*, 2023, **333**, 126363.

23 M. Ghazimoradi, S. Soltanali, H. Karami, H. Ghassabzadeh and J. Bakhtiari, *RSC Adv.*, 2023, **13**, 20058.

24 M. Ghazimoradi, S. Soltanali, N. Safari and H. Ghassabzadeh, *J. Mater. Sci.*, 2023, 1–17.

25 S. Li, A. Liutkova, N. Kosinov and E. J. M. Hensen, *ACS Appl. Nano Mater.*, 2022, **5**, 16862–16871.

26 E. N. Al-Shafei, M. Z. Albahar, M. F. Aljishi, A. N. Aljishi, G. A. Nasser, M. A. Sanhoob, A. S. Alnasir and A. AlAsseel, *Fuel*, 2022, **321**, 124089.

27 M. Ghazimoradi, N. Safari, S. Soltanali and H. Ghassabzadeh, *Microporous Mesoporous Mater.*, 2023, 112486.

28 Z. Wan, W. Wu, G. K. Li, C. Wang, H. Yang and D. Zhang, *Appl. Catal., A*, 2016, **523**, 312–320.

29 A. Dubey, A. Singh, A. Sharma, A. K. Sundramoorthy, R. Mahadeva, V. Gupta, S. Dixit and S. Arya, *Appl. Phys. A: Mater. Sci. Process.*, 2023, **129**, 692.

30 H. Karami and S. Soltanali, *Surf. Interfaces*, 2023, 103813.

31 Y. Tavan, M. R. K. Nikou and A. Shariati, *J. Ind. Eng. Chem.*, 2014, **20**, 668–673.

32 M. A. Sanhoob, O. Muraza, M. Yoshioka, M. Qamaruddin and T. Yokoi, *J. Anal. Appl. Pyrolysis*, 2018, **129**, 231–240.

33 M. S. Aghdam, S. Askari, R. Halladj and A. F. Tajar, *Adv. Powder Technol.*, 2022, **33**, 103502.

34 F. M. Shalmani, R. Halladj and S. Askari, *RSC Adv.*, 2017, **7**, 26756–26769.

35 L. N. Vosmerikova, Y. E. Barbashin and A. V Vosmerikov, *Pet. Chem.*, 2014, **54**, 420–425.

36 F. Rahmani, M. Haghighi and P. Estifaee, *Microporous Mesoporous Mater.*, 2014, **185**, 213–223.

37 G. Lawes, J. Goldstein, D. E. Newbury, P. Echlin, D. C. Joy, A. D. Romig Jr, C. E. Lyman, C. Fiori and E. Lifshin, *Scanning Electron Microscopy and X-Ray Microanalysis: A Text for Biologists, Materials Scientists, and Geologists*, Springer, 1992.

38 X. Wei and P. G. Smirniotis, *Microporous Mesoporous Mater.*, 2006, **97**, 97–106.

39 X. Zhang, D. Cheng, F. Chen and X. Zhan, *Chem. Eng. Sci.*, 2017, **168**, 352–359.

40 H. Karami, M. Kazemeini, S. Soltanali and M. Rashidzadeh, *Can. J. Chem. Eng.*, 2022, **11**, 3357–3366.

41 H. Karami, M. Kazemeini, S. Soltanali and M. Rashidzadeh, *Microporous Mesoporous Mater.*, 2022, **332**, 111704.

42 S. Hassanpour, M. Taghizadeh and F. Yaripour, *Ind. Eng. Chem. Res.*, 2010, **49**, 4063–4069.

43 H. Karami, S. Soltanali, A. M. Najafi, M. Ghazimoradi, E. Yaghoobpour and A. Abbasi, *Appl. Catal., A*, 2023, **658**, 119167.

44 W.-Z. Lang, C.-L. Hu, L.-F. Chu and Y.-J. Guo, *RSC Adv.*, 2014, **4**, 37107–37113.

45 S. Askari, R. Halladj and M. Sohrabi, *Microporous Mesoporous Mater.*, 2012, **163**, 334–342.

46 P. Sadeghpour and M. Haghighi, *Adv. Powder Technol.*, 2018, **29**, 1175–1188.

47 X. Jiang, X. Su, X. Bai, Y. Li, L. Yang, K. Zhang, Y. Zhang, Y. Liu and W. Wu, *Microporous Mesoporous Mater.*, 2018, **263**, 243–250.

48 M. A. Sanhoob, O. Muraza, T. Tago, T. Taniguchi, G. Watanabe and T. Masuda, *Res. Chem. Intermed.*, 2016, **42**, 6437–6448.

49 M. A. Sanhoob, E. N. Shafei, A. Khan, G. A. Nasser, I. Bakare, O. Muraza, M. Z. Al-Bahar, A. N. Al-Jishi, H. H. Al-Badairy and A. C. Ummer, *ACS Omega*, 2022, **7**, 10317–10329.

50 D. He, Y. Zhang, S. Yang, Y. Mei and Y. Luo, *ChemCatChem*, 2018, **10**, 5434–5440.

51 O. D. A. Salah Aldeen, M. Z. Mahmoud, H. S. Majdi, D. A. Mutlak, K. Fakhriddinovich Uktamov and E. Kianfar, *Adv. Mater. Sci. Eng.*, 2022, **2022**, 6165180.

52 H. Li, B. Zhu, D. Wang, S. Fan, X. Gao, J. Zhang, Q. Ma and T. Zhao, *Microporous Mesoporous Mater.*, 2021, **327**, 111403.